Comparison of Field-scale Effective Properties of Two-phase Flow in Heterogeneous Porous Media Obtained by Stochastic Analysis and Numerical Experiments

Quanlin Zhou

Earth Sciences Division, Lawrence Berkeley National Laboratory, Berkeley, California

Lynn W. Gelhar

Department of Civil & Environmental Engineering, Massachusetts Institute of Technology, Cambridge, Massachusetts

Bruce Jacobs

Jacobs Consulting Services, Boston, Massachusetts

Abstract

The effects of subsurface heterogeneity on two-phase flow can be observed from the characterization functions of field-scale effective relative permeability and capillary pressure with respect to mean saturation. Numerical experiments were used to evaluate such effective properties of two-phase flow in a heterogeneous medium with properties representing the Borden Aquifer, and compared with the results of stochastic analysis developed using a spectral perturbation technique that employs a stationary, stochastic representation of the spatial variability of soil properties. Arbitrary forms of the relative permeability and capillary pressure characteristic functions with respect to saturation can be used in the theoretical analysis and numerical code. A statistical scaling procedure, which is a generalization of Leverett scaling, was developed for the relationship between intrinsic permeability and two capillary parameters.

The procedure for estimating the effective properties of two-phase flow using numerical simulation consists of three-steps. Firstly, a local-scale heterogeneous system with random fields of intrinsic permeability and two capillary parameters was generated. Secondly, numerical simulation of single-phase flow in the system, with different sets of flow boundary conditions for different directions, was performed; the field-scale effective saturated hydraulic conductivity tensor was calculated on the basis of the mean Darcy law. The tensor obtained numerically is very close to that determined using the generalized spectral-perturbation approximation. Finally, a number of numerical experiments on two-phase flow in the system were conducted with different infiltration rates of DNAPL; the field-scale effective relative permeability and capillary pressure functions were obtained. In each experiment, a highly heterogeneous saturation field was obtained, leading to large variations of actual nonwetting phase permeability (combination of intrinsic permeability and its positively correlated relative permeability).

Both stochastic and numerical analyses produced very similar results of effective properties of multiphase flow. The vertical effective relative permeability is significantly lower than the homogeneous one found using mean capillary parameters, particularly at low mean DNAPL saturation (low mean capillary pressure). On the other hand, the effective capillary pressure function differs only slightly from the homogeneous case. Various statistical properties of local-scale NAPL saturation, capillary pressure and

relative permeability and their relationships with intrinsic permeability and capillary parameters were analyzed in detail.

1. Introduction

The widespread subsurface contamination by dense nonaqueous phase liquids (DNAPLs) has posed serious environmental and health hazards worldwide. DNAPLs usually exhibit low aqueous solubility and relative inaccessibility in natural formations. As a result, they represent a highly persistent source of environmental contamination, posing unique challenges to environmental remediation efforts. Heterogeneity in natural formations has been demonstrated to have a significant influence on DNAPL migration in the unsaturated and saturated zones. Such an influence depends on the variability of capillary parameters, which are scaled to the primary heterogeneous variable: intrinsic permeability.

The spectral perturbation technique has been applied to investigate field-scale effective functions of capillary pressure and relative permeability with respect to saturation in the unsaturated and saturated zones. *Yeh et al.* [1985] estimated the effective properties of steady unsaturated flow by assuming that the dependence of relative permeability on capillary pressure is of exponential form. *Jacobs* [1999] derived the effective properties of the nonwetting phase in two-phase flow, with high flexibility of selection of arbitrary functional forms of the local characterization of capillary pressure, saturation and relative permeability. He found that the anisotropy of effective NAPL relative permeability increases with increasing mean effective water saturation. In a DNAPL-water system, the variance of local-scale actual hydraulic conductivity of nonwetting phase is large, even in a mildly heterogeneous formation. Since the terms higher than first order are truncated in the spectral-perturbation analysis, the spectral-perturbation technique can be used only for heterogeneous systems with small variance of intrinsic permeability and capillary parameters.

The goal of the paper is to investigate the field-scale effective properties of two-phase flow in a heterogeneous system through numerical simulation and compare the results with the theoretical ones obtained by *Jacobs* [1999] using the spectral perturbation method. In Section 2, the mathematical model for two-phase flow and a statistical scaling technique are presented. A heterogeneous system with random fields of intrinsic permeability and two capillary parameters is generated using a fast Fourier transform generator in Section 3. In Section 4, the effective saturated hydraulic conductivity was derived on the basis of the simulation results of single-phase flow in the heterogeneous system. In Section 5, the effective properties of two-phase flow were obtained through a number of two-phase flow simulations with different DNAPL infiltration rates. Both numerical results of effective saturated hydraulic conductivity of single-phase flow and effective properties of two-phase flow were compared with their theoretical counterparts using the spectral perturbation method.

2. Mathematical and Numerical Model

2.1. Governing Equations

The flow equations for the wetting and nonwetting phases can be written in terms of water and NAPL heads:

$$\frac{\partial \phi S_w}{\partial t} = \frac{\partial}{\partial x_i}\left(K_{ij}^w k_{rw} \frac{\partial h_w}{\partial x_j} \right), \tag{1}$$

$$\frac{\partial \phi S_n}{\partial t} = \frac{\partial}{\partial x_i}\left(K_{ij}^n k_{rn} \frac{\partial h_n}{\partial x_j} \right), \tag{2}$$

with

$$K_{ij}^w = \rho_w g k_{ij} / \mu_w , \qquad K_{ij}^n = \rho_w g k_{ij} / \mu_n = K_{ij}^w / R_\mu$$

where ϕ is the porosity, the subscripts w, n represent the wetting (water) and nonwetting (DNAPL) phases, respectively, S_γ is the saturation of the γ phase ($\gamma = w, n$), k_{ij} is the intrinsic permeability tensor, ρ_γ is the fluid density, μ_γ is the dynamic viscosity, $k_{r\gamma}$ is the relative permeability, K_{ij}^w is the saturated hydraulic conductivity tensor of the wetting phase, K_{ij}^n is the saturated hydraulic conductivity tensor of the nonwetting phase, h_w is the water head ($h_w = P_w / \rho_w g + z$), h_n is the nonwetting phase (NAPL) head ($h_n = P_n / \rho_w g + z$), P_γ is the fluid pressure, R_ρ is the density difference ratio ($R_\rho = (\rho_n - \rho_w)/\rho_w$), R_μ is the dynamic viscosity ratio ($R_\mu = \mu_n / \mu_w$), x_i is the Cartesian coordinates, z is the vertical component of x_i, and t is the time. These equations are coupled through the capillary pressure relationship

$$h_n = h_w + h_c(S_n) + R_\rho z , \tag{3}$$

and are subject to

$$S_w + S_n = 1, \tag{4}$$

where $h_c(S_n)$ is the capillary head ($h_c = P_c / \rho_w g$) dependent on NAPL saturation, and P_c is the capillary pressure.

2.2. Capillary Scaling

Capillary pressure scaling has been demonstrated to have significant influence on the investigation of DNAPL migration in heterogeneous porous media by various numerical simulators [e.g., *Kueper and Frind*, 1991]. *Jacobs* [1999] presented a *statistical scaling technique*, in which both the deterministic correlation between capillary parameters (e.g., α^{-1} and m in the van Genuchten formulation) and permeability and random perturbations are considered. The scaling method can be written

$$F = \overline{F} + f\,, \tag{5a}$$

$$B = \overline{B} + b_B f + g_B\,, \tag{5b}$$

$$L = \overline{L} + b_L f + g_L\,, \tag{5c}$$

with the definition of

$$F = \ln K^w\,,$$

$$B = \ln \alpha^{-1}\,,$$

$$L = -\ln(1/m - 1)\,,$$

where f, g_B, g_L are the statistically independent perturbations of zero mean, b_B and b_L are the correlation parameters determined from measured data, and the bar over a variable indicates its mean value. The modified *Leverett* scaling can be considered as a special case of the statistical scaling in that the slope parameter is constant and the best-fit exponent is identical to the correlation $-b_B$.

2.3. Numerical Simulator

The FEAS-MPFLOW code was developed for simulating two-phase flow. This code is a member of a C++ code family (called as FEAS) for the Finite Element Aquifer Simulation of subsurface flow, contaminant, and heat transport. The Galerkin finite element method is used to discretize the governing equation(s). In the FEAS-MPFLOW code, water head, h_w, and NAPL saturation, S_n, are selected as primary variables.

Considering that the advection-type gravity force works differently from the diffusion-type capillary and water head gradients, an upstream scheme is employed only for the relative permeability in estimating the gravity term. This special upstream scheme works well for homogeneous and heterogeneous media.

Nodal permeability and capillary parameters are employed in the FEAS-MPFLOW. Thus, material properties are continuous within a whole solution domain, as well as the primary and secondary variables, like capillary pressure. This treatment is introduced because in the standard finite element method, the element-wise material properties lead to discontinuity of saturation along element interfaces in heterogeneous media.

3. Random Fields of Permeability and Capillary Parameters

The *statistical scaling technique* presented by *Jacobs* [1999] was combined with a fast Fourier transform field generator [*Ruan and McLaughlin*, 1998] for generating a heterogeneous system with random fields of intrinsic permeability and capillary parameters. The two-dimensional random fields of the transformed *F*, *B*, and L were generated simultaneously based on (5). It is assumed there are no significant trends in the large-scale mean process of F, B and L; the hole-type covariance function is suitable for the spatial statistical correlation of logarithm of intrinsic permeability; perturbations

g_B and g_L have the same covariance function as perturbation *f;* and g_B, g_L and f are statistically independent.

The statistical properties representing the Borden Aquifer were used to generate the random fields. The correlation scales (λ_x and λ_z) are 2.8 m and 0.12 m in the horizontal and vertical directions, respectively [*Sudicky*, 1986; *Jacobs*, 1999]; other related parameters are: $\overline{F} = -9.5114$ (*ln*m/s), $\overline{B} = -1.0937$ (*ln*m), $\overline{L} = 1.50$, $\sigma_f = 0.351$, $b_B = -1.03$, $\sigma_{g_B} = 0.113$, $b_L = -0.83$, and $\sigma_{g_L} = 0.174$, where σ indicates the standard deviation of a random variable of interest. These parameter values were calculated [*Jacobs*, 1999] on the basis of seven samples of capillary head and saturation curve from field measurement obtained by *Kueper and Frind* [1991].

The heterogeneous domain is $8\lambda_x$ long and $16\lambda_z$ high in the two-dimensional vertical cross-section. Uniform spatial discretizations in the horizontal and vertical directions are $\lambda_x/16$ ($\Delta x = 0.175m$) and $\lambda_z/4$ ($\Delta z = 0.03m$). The grid for random field generation consists of 128×64 nodes. The generated values of *F*, *B*, and *L* are set at grid nodes, rather than at the centroids of finite elements or cells.

The statistical properties of the generated fields of *F*, *B* and *L* in the whole solution domain agree very well with their input parameters. Obvious layering of low and high intrinsic permeability is observed in the generated permeability field. This is due to the high ratio of the horizontal correlation scale to the vertical one. A highly negative correlation between the generated characteristic capillary head (α^{-1}) and the intrinsic permeability is observed. We can also see a highly negative correlation between the generated slope parameter (*m*) and the intrinsic permeability. The covariance functions in the horizontal and vertical directions, estimated from the generated *F* field, are also in good agreement with their theoretical covariance functions.

4. Effective Saturated Hydraulic Conductivity

The first step in determining the field-scale effective relative permeability in heterogeneous formations is to estimate the field-scale effective saturated hydraulic conductivity tensor ($\mathbf{K}_s^e$). This tensor is of non-zero diagonal terms and of zero off-diagonal ones for a local-scale isotropic medium [*Gelhar*, 1993]. We employ two different flow situations in the generated heterogeneous system, and estimate each component of $\mathbf{K}_s^e$ by simulating steady-state single-phase flow in their corresponding flow situation.

Let us first determine the vertical component, K_{sz}^{ew}, of effective saturated hydraulic conductivity for water flow. The generated heterogeneous domain is employed here as the solution domain. The left and right side boundaries are impervious to single-phase (water) flow. A constant recharge rate of $q_z = 1 \times 10^{-5} m/s$ is specified at the top boundary, and a constant water head is specified at the bottom, where the injected water is allowed to flow out. The generated nodal permeability field is used as parameter input, and the grid for the generation of random fields is used for the computational mesh.

The component of effective saturated hydraulic conductivity in the vertical direction was estimated on the basis of the mean Darcy law. The mean values of specific discharge and hydraulic gradient were obtained by simulating the single-phase flow in the flow situation set up above.

Similarly, we change the boundary conditions for calculating the horizontal component of the effective saturated hydraulic conductivity as follows: the top and the bottom are impervious to water flow; a constant rate of water ($q_x = 1\times10^{-5} m/s$) is injected from the left-hand-side boundary; a constant head is specified on the right-hand-side boundary.

Table 1. Comparison of effective saturated hydraulic conductivity tensors obtained by the present numerical simulation and spectral-perturbation analysis.

		Vertical	Horizontal
Numerical	$K_{sx_j}^{ew}$ ($\times10^{-5} m/s$)	7.202	7.925
Spectral	$\overline{K_{sx_j}^{w}}$ ($\times10^{-5} m/s$)	7.150	7.888

The estimated effective saturated conductivity tensor is presented in Table 1. For comparison, the generalized spectral-perturbation approximation of effective hydraulic conductivity in two-dimensional anisotropic (for the correlation scales) formations is also presented in Table 1 [*Gelhar*, 1993]. The approximation for the horizontal and vertical effective conductivity for the generated permeability field can be written

$$\overline{K_{sx}^{w}} = K_g^* \exp\left(\sigma_f^{*2}\left(\frac{1}{2} - \frac{\lambda_z}{\lambda_x + \lambda_z}\right)\right), \tag{6a}$$

$$\overline{K_{sz}^{w}} = K_g^* \exp\left(\sigma_f^{*2}\left(\frac{1}{2} - \frac{\lambda_x}{\lambda_x + \lambda_z}\right)\right), \tag{6b}$$

where K_g^* and σ_f^* are the geometric mean of local-scale hydraulic conductivity and standard deviation of F computed over the generated system.

The horizontal and vertical components of the present effective saturated conductivity tensor agree very well with their corresponding spectral-perturbation approximations. Both estimations of the vertical component are smaller than the geometric mean of the generated hydraulic conductivity field ($K_g^* = 7.518\times10^{-5} m/s$). This is due to the significant effect of harmonic averaging, as the horizontal correlation scale is much larger than the vertical one.

5. Effective Relative Permeability and Capillary Pressure Functions

The field-scale effective properties (effective relative permeability and capillary pressure functions) of two-phase flow involve the influence of local-scale heterogeneity of natural formations. The field-scale effective NAPL relative permeability is defined as the ratio of effective actual hydraulic conductivity of nonwetting phase to its corresponding effective saturated conductivity obtained in Section 4. By excluding the effects of heterogeneity of intrinsic permeability on the effective saturated conductivity, the effective relative permeability is expected to represent the effects of variability of capillary parameters alone. The effective relative permeability exhibits anisotropy in natural formations, even for the local-scale isotropic intrinsic permeability. In the paper, only the vertical effective relative permeability is presented. The effective capillary pressure function in terms of mean saturation and mean capillary pressure is also obtained by numerical simulation. Our goal here is to estimate the field-scale effective properties by simulating two-phase flow in the generated heterogeneous system with random fields of capillary parameters and intrinsic permeability.

5.1. Numerical simulation

The generated heterogeneous domain is employed as the solution domain. The boundary conditions for the two-phase flow system are presented as follows. Both the left- and right-hand side vertical boundaries are impervious to water and DNAPL flow. On the top boundary, a constant rate of DNAPL, q_z^*, is injected into the flow system, with no flow of the wetting phase. On the bottom boundary, a constant water head is specified and a solution-dependent DNAPL flux is specified to allow for outflow of the nonwetting phase liquid. This flux rate, determined by neglecting the effects of gradients of water and capillary heads, is related only to the gravity driving force. A uniform initial DNAPL saturation field is specified for a specified infiltration rate, q_z^*.

The generated fields of nodal intrinsic permeability and capillary parameters are employed for parameter input. The medium porosity is 0.35 and water residual saturation is 0.1. The density of water and DNAPL is 1000 and 1600 kg/m^3 respectively, leading to $R_\rho = 0.60$. The dynamic viscosity of water and DNAPL is 0.001 and 0.0005 kg/ms, and the viscosity ratio is $R_\mu = 0.5$. Nine flow situations with different specified infiltration rates ($q_z^* = 5000,\ 2000, 1000, 500, 200, 50, 20, 10, 1\times10^{-8}\ m/s$) on the top boundary were simulated, in order to obtain the effective relative permeability and capillary pressure functions with respect to mean effective saturation (μ_{S_e}). For each infiltration case, the transient process of DNAPL transport was simulated until a quasi-steady-state was reached.

5.2. Spectral Analysis of Effective Properties

For comparison, we briefly present the spectral-perturbation analysis. This analysis is performed on steady-state systems of two fluid phases with significant density differences such that gravitational forces are likely to be the primary factor in determination of the mean flow direction. Soil properties are represented as a stationary,

spatially correlated random field whose statistical properties are measured from direct observation. The hole-type of covariance function and the statistical properties given in previous sections are also used here. The spatial distribution of a random variable (a soil property or a system output variable, such as hydraulic head and capillary pressure head) is represented as the composite of two independent signals: a large-scale slowly varying deterministic mean and high frequency random perturbation.

In the first step, the field-scale effective properties (effective relative permeability, effective capillary pressure and mean saturation) are derived in terms of the mean, variance and covariance of the local-scale input variables (F, B, L), and output variables (hydraulic head gradient $J_i^\gamma (\equiv \partial h_\gamma / \partial x_i)$ and capillary pressure h_c). The Darcy law can be written:

$$q_i^\gamma = \frac{\exp(R_\gamma(\Gamma))}{\mu_\gamma} J_i^\gamma, \; R_\gamma(\Gamma) = \ln(k k_\gamma), \tag{7}$$

where Γ is a parameter vector $\{F, B, L, h_c\}$. The function R_γ is linearized using Taylor expansion of nonlinear terms about the mean of their parameters. Then, the head gradients and the vector of parameters are represented by their means and perturbations. Finally, taking the expected value of the resulting expression leads to the expression for effective field-scale permeability. The effective field-scale relative permeability is obtained as the ratio of the effective field-scale permeability to the effective saturated permeability, which is a function of only the intrinsic permeability (F).

In the second step, the mean cross products of output and input variables are determined by the solution of the stochastic differential equation (SDE) for multiphase flow. First, the SDE is linearized substituting the sum of the mean and perturbation for each of the random variables and performing a Taylor expansion $R_\gamma(\Gamma)$ at $\bar{\Gamma}$. Second, the mean equation is found by taking the expected value of the linearized SDE, while neglecting terms exceeding second-order. Third, the governing equation of the random perturbation quantities (perturbation equation) is found by subtracting the mean equation from the linearized SDE. The perturbation equation is written in the wave number domain as in Gelhar [1993]. The cross-spectra expressions for cross-products of input and output variables are derived to evaluate the effective properties.

The effective relative permeability and effective capillary pressure can be evaluated for any flow condition with the above assumptions by evaluating integrals of the cross spectra. Jacobs [1999] estimated the effective properties by analytically evaluating the cross-product integrals for the condition of uniform flow perpendicular to the principal axes and the condition of perfectly stratified aquifer. For any other flow conditions, numerical integration is required for evaluating these integrals of cross-spectra. For the current case, the numerical integration is used and the results are presented in Figures 1-4.

5.3. Properties of NAPL Saturation Field

For each flow situation or infiltration rate, a quasi-steady NAPL saturation field with large variation was obtained, representing the overall influence of variability of the intrinsic permeability and the capillary parameters. The NAPL saturation field exhibits the following statistical properties:

1. The standard deviation of NAPL saturation ($\sigma_{S_n}(\mu_{S_e})$) increases from zero at fully NAPL-saturated conditions to its peak at the mean effective saturation of $\mu_{S_e} = 0.5$, and then decreases as μ_{S_e} approaches the fully water-saturated status as shown in Figure 1.
2. The auto-covariance function of saturation in the vertical direction, shown in Figure 2a, varies with mean saturation. The correlation scale of saturation is less than that of the logarithm of intrinsic permeability ($= 2.31\lambda_z$). This scale increases with mean effective saturation until it reaches its peak at about $\mu_{S_e} = 0.5$, then it decreases with increases in μ_{S_e}.
3. The NAPL saturation field is *positively correlated* with the primary intrinsic permeability field, as shown in Figure 2b. This positive correlation mainly comes from the negative correlation between the characteristic capillary pressure α^{-1} and the intrinsic permeability. The correlation coefficient decreases with increasing μ_{S_e} in the range of μ_{S_e} of numerical simulation, as shown in Figure 2b and c.

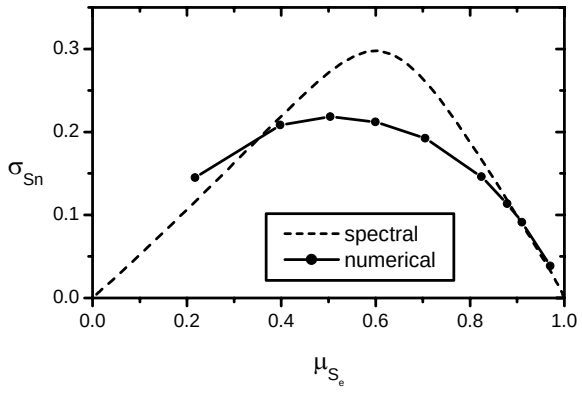

Figure 1. Comparison of standard deviation of NAPL saturation between numerical and spectral analysis.

Figure 1 shows the standard deviation of NAPL saturation obtained numerically in comparison with the theoretical spectral-analysis approximation [Jacobs, 1999]. A small difference occurs in the middle range of μ_{S_e}, with the maximum of 0.100 at $\mu_{S_e} = 0.60$. With increase in μ_{S_e}, the agreement becomes excellent. Figure 2c shows that the correlation coefficients obtained by numerical and spectral analyses have similar

trend with respect to μ_{S_e}. There exists good agreement in the cross-covariance function, $\mathrm{cov}(S_n, f)$, between numerical and spectral analysis, as shown in Figure 2b and d.

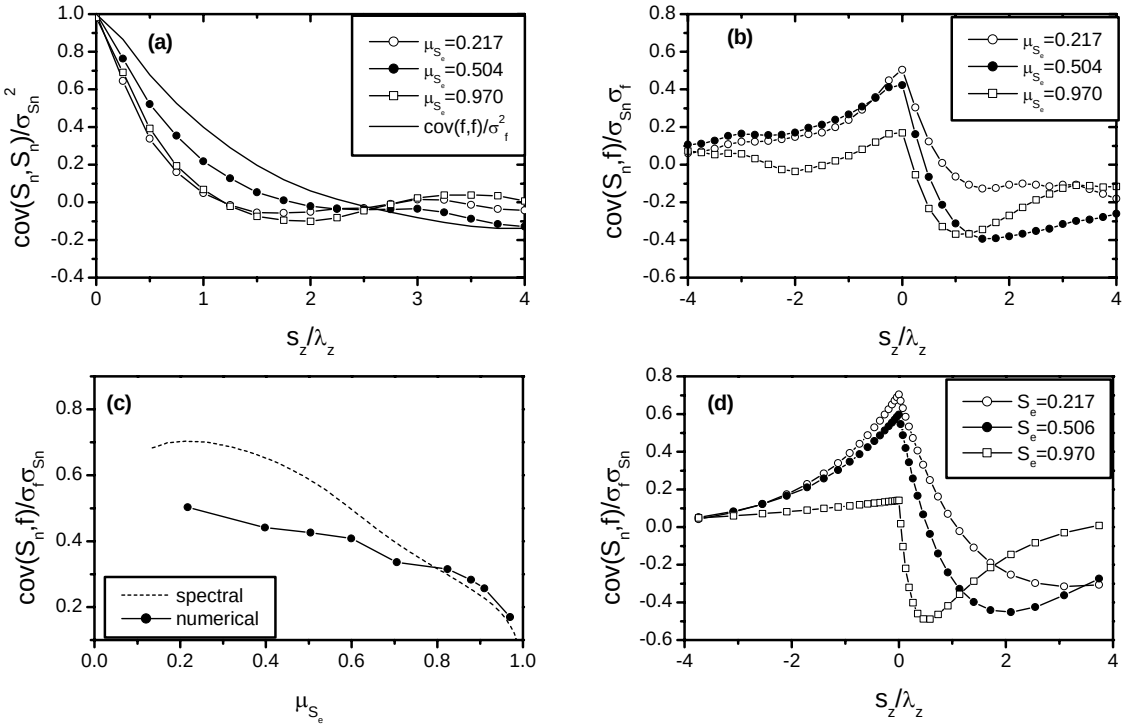

Figure 2. Variations of (a) autocovariance function of NAPL saturation, (b) cross-covariance of NAPL saturation with log intrinsic permeability, (c) correlation coefficient of NAPL saturation and *f*, and (d) cross-covariance function of NAPL saturation with *f* obtained by spectral analysis..

5.4. Effective Relative Permeability

The mean Darcy's law for the nonwetting phase liquid is employed for estimating the effective relative permeability in the vertical direction (k_{rz}^{en}):

$$k_{rz}^{en} = \frac{\overline{q_z^n}}{K_{sz}^{en}\,\overline{J_z^{h_n}}}, \tag{8}$$

where $\overline{q_z^n}$ is the mean vertical component of specific discharge vector, $\overline{J_z^{h_n}}$ is the mean hydraulic gradient of the nonwetting phase liquid in the vertical direction, and K_{sz}^{en} is the effective saturated hydraulic conductivity of NAPL ($K_{sz}^{en} = K_{sz}^{ew} / R_\mu$). The mean effective saturation, μ_{S_e}, was obtained by averaging the nodal effective saturation field over the

solution domain. For a given infiltration rate, a pair of effective relative permeability and mean saturation, (k_{rz}^{en}, μ_{S_e}), was obtained.

Figure 3a shows the vertical effective relative permeability (k_{rz}^{en}) obtained by numerical simulation, in comparison with the approximation of spectral-perturbation analysis (k_{rz}^{nS}) and the homogeneous one ($k_{rn}(\overline{m})$) with mean capillary parameters. The computed k_{rz}^{en} for each infiltration case is smaller than its corresponding homogeneous one. The ratio of $k_{rz}^{en}/k_{rn}(\overline{m})$ gradually decreases from 1.0 at $\mu_{S_e}=0$ to the value of 0.068 at $\mu_{S_e}=0.970$. The difference between k_{rz}^{en} and $k_{rn}(\overline{m})$ represents the effects of heterogeneity of capillary parameters. It is also shown that the present effective relative permeability is close to k_{rz}^{nS}, which is obtained by spectral-analysis [*Jacobs*, 1999].

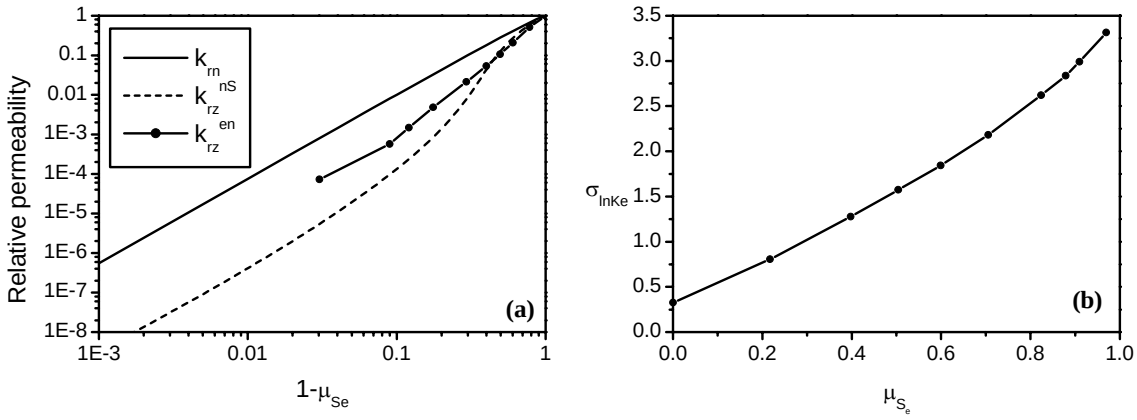

Figure 3. (a) Comparison of the vertical effective relative permeability obtained by numerical simulation and spectral analysis, and (b) standard deviation of natural logarithm of actual conductivity.

The reasons for the above findings for vertical effective relative permeability can be explained from the following two major points.

1. The local-scale relative permeability of the nonwetting phase is *positively correlated* with intrinsic permeability. The cross-covariance function between $\ln(k_{rn})$ and $\ln(K_s^n)$ is similar to that between S_n and $\ln(K_s^n)$ shown in Figure 2b. This means that the variation in NAPL saturation dominates that of the relative permeability. For a layer of low permeability, the relative permeability $k_{rn}(S_n)$ is also small due to the low NAPL saturation. In addition, the correlation coefficient decreases with increase in μ_{S_e} in the range of μ_{S_e} of numerical simulation.

2. Large standard deviations of log actual hydraulic conductivity, $\ln(K_e^n)$, of the nonwetting phase are shown in Figure 3b. At $\mu_{S_e}=0$ and $\mu_{S_e}=1$, the relative permeability is equal to 1.0, and the variance of hydraulic conductivity stems

solely from variance of intrinsic permeability. When both phases are present in the considered domain, the variance of relative permeability contributes to large variation of the actual hydraulic conductivity.

5.5. Effective Capillary Pressure Function

Figure 4a shows the effective capillary head function for the considered heterogeneous system in comparison with that obtained by the spectral-perturbation analysis [Jacobs, 1999] and that for the homogeneous case. The deviation in the effective capillary head from the homogeneous one is very small, in particular for a high μ_{S_e}. With the decrease in μ_{S_e}, such a deviation slightly increases, as the capillary head variance increases. This small deviation may result from the small variance of the capillary head field shown in Figure 4b. The standard deviation of capillary head, σ_{h_c}, is smaller than both σ_{S_n} and $\sigma_{\alpha^{-1}}$. This stems from the negative correlation between S_n and α^{-1} discussed above. The standard deviation increases with μ_{S_e} until it reaches its maximum around $\mu_{S_e} = 0.5$, and then decreases, as shown in Figure 4b. The agreement between the present numerical effective capillary pressure and that obtained by the spectral-perturbation analysis is very good. The standard deviation curves of capillary head in Figure 4b show that both the numerical and spectral curves are close in magnitude, although there is some difference in the shapes of curves.

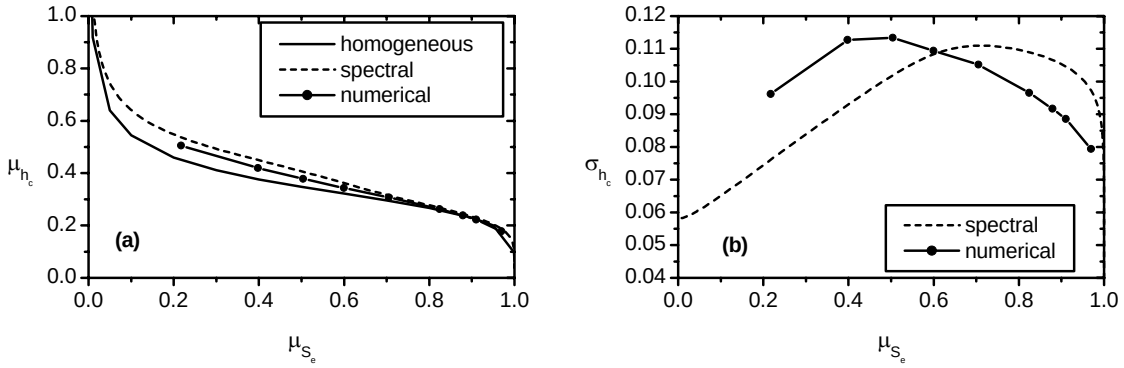

Figure 2. Comparison of (a) effective capillary head function and (b) standard deviation of capillary head obtained by numerical and spectral analysis.

6. Conclusion

The field-scale effective relative permeability and capillary pressure function (with respect to mean saturation) of two-phase flow were obtained using numerical and stochastic analysis. The difference between such effective properties in a heterogeneous formation and those in a homogeneous formation with mean local-scale properties represents the effect of subsurface heterogeneity. In the numerical analysis, a heterogeneous system with random fields of intrinsic permeability and two capillary

pressure parameters (representing the Borden Aquifer) was generated using the statistical capillary scaling. The effective saturated hydraulic conductivity was estimated by simulating the single-phase water flow in the heterogeneous system. The field-scale effective properties of two-phase flow for the heterogeneous system were estimated through numerical simulations of two-phase water-DNAPL flow with different mean saturation. The effective relative permeability was calculated on the basis of the mean Darcy law. For comparison, stochastic analysis was also employed using a spectral perturbation technique, which employs a stationary, stochastic representation of the spatial variability of soil properties.

The field-scale effective saturated hydraulic conductivity tensors obtained by numerical and stochastic analysis agree very well. The vertical effective relative permeability is significantly lower than the homogeneous one found using mean capillary parameters, particularly at low mean DNAPL saturation (low mean capillary pressure). The significant difference is mainly due to the large variance of actual DNAPL permeability (combination of intrinsic permeability and its positively correlated relative permeability). On the other hand, the effective capillary pressure function differs only slightly from the homogeneous case. This deviation results from the small variance of capillary pressure, which is smaller than that of the capillary parameters. By comparison, the effective properties of two-phase flow obtained by the numerical simulation and stochastic analysis are in good agreement. The numerical analysis can be used for any highly heterogeneous formations, whereas the stochastic analysis can give us insight into the internal correlations between output and input variability in mildly heterogeneous systems.

References

1. Gelhar, L. W., *Stochastic subsurface hydrology*, Prentice Hall, Englewood Cliffs, NJ, 1993.
2. Jacobs, B. L., Effective properties of multiphase flow in heterogeneous porous media, Ph.D. thesis, Massachusetts Institute of Technology, 1999.
3. Kueper, B. H., and E. O. Frind, Two-phase flow in heterogeneous porous media: 2. model application, *Water Resour. Res.*, 27(6), 1059-1070, 1991.
4. Ruan, F., and D. McLaughlin, An efficient multivariate random field generator using the fast Fourier transform, *Adv. Water Resour.*, 21, 385-399, 1998.
5. Sudicky, E. A., A natural gradient experiment on solute transport in a sand aquifer: spatial variability of hydraulic conductivity and its role in the dispersion process, *Water Resour. Res.*, 22(13), 2069-2082, 1986.
6. Yeh, T-C. J., L. W. Gelhar, and A. L. Gutjahr, Stochastic analysis of unsaturated flow in heterogeneous soils: 1. statistically isotropic media, *Water Resour. Res.*, 21(4), 447-456, 1985.